A Spectral Element Projection Scheme for Incompressible Flow With Application to Shear-Layer Stability Studies

F.N. van de Vosse* P.D. Minev† L.J.P. Timmermans‡

Abstract

A projection scheme based on the pressure correction method is discussed to solve the Navier–Stokes equations for incompressible flow. The algorithm is applied to the continuous equations, imposing a proper boundary condition on the pressure correction step. The resulting velocity and pressure satisfy the original equations, except for the tangential boundary condition for the velocity, which is satisfied with second-order accuracy in time. For the spatial discretization the spectral element method is chosen. The high-order accuracy allows the use of a diagonal mass matrix resulting in a very efficient algorithm. The scheme is applied for simulating shear-layer flow. Proper outflow conditions are formulated in terms of the unknowns of the decoupled system. These conditions seem to be suitable for non-parallel outflows, not causing any severe stability problems.

Key words:
spectral element method, projection method, shear-layer flow.

AMS subject classifications: 65N30, 76F10, 65N35.

*Department of Mechanical Engineering, Eindhoven University of Technology, P.O. Box 513, 5600 MB Eindhoven, The Netherlands

†Stevin Center for Computational and Experimental Engineering Science, Eindhoven University of Technology, P.O. Box 513, 5600 MB Eindhoven, The Netherlands

‡Department of Mechanical Engineering, Eindhoven University of Technology, P.O. Box 513, 5600 MB Eindhoven, The Netherlands (present address: Laboratory for Aero- and Hydrodynamics, Delft University of Technology, Rotterdamseweg 145, 2628 AL Delft, The Netherlands)

ICOSAHOM'95: Proceedings of the Third International Conference on Spectral and High Order Methods.

1 Introduction

Calculating the solution of the Navier–Stokes equations for unsteady incompressible fluid flow is still a major challenge in the field of computational fluid dynamics. The Navier–Stokes equations form a set of coupled equations for both velocity and pressure (or, better, the gradient of the pressure). One of the main problems related to the numerical solution of these equations is the imposition of the incompressibility constraint and, consequently, the calculation of the pressure. The pressure is not a thermodynamic variable as there is no equation of state for an incompressible fluid. It is an implicit variable which instantaneously 'adjusts itself' in such a way that the velocity remains divergence-free. The gradient of the pressure, on the other hand, is a relevant physical quantity: a force per unit volume. The mathematical importance of the pressure in an incompressible flow lies in the theory of saddle-point problems (of which the steady Stokes equations are an example), where it acts as a Lagrangian multiplier that constrains the velocity to remain divergence-free [3].

For the solution of unsteady Navier–Stokes flow, perhaps one of the most successful approaches to-date is provided by the class of projection methods [2], [5]. Projection methods have been developed as a useful way to obtain an efficient solution algorithm for unsteady incompressible flow. In this paper, projection methods are considered that are applied to the set of continuous equations, yielding methods for implementing algorithms. By decoupling the treatment of velocity and pressure terms, a set of easier-to-solve equations arises: a convection-diffusion problem for the velocity, yielding an intermediate velocity which is not divergence-free; and a Poisson equation for the pressure (or a related quantity). There are, essentially, two approaches for continuous projection methods: fractional step methods and pressure correction methods.

The fractional step method [11], [12], is based on a full splitting of the treatment of the pressure/incompressibility constraint and the diffusion in different sub-steps. The intermediate step leads to a Poisson equation for the pressure at the new time-level. While the pressure is well-defined

up to an arbitrary constant by the original equations, it is less so when directly expressed in terms of a Poisson equation. This is because, in the latter case, the necessity arises to formulate a non-trivial boundary condition for the pressure. The choice of the pressure boundary condition is an aspect that is much discussed in literature [4], [11], [18]. The obvious theoretical choice for the pressure boundary condition is a Neumann condition derived from the normal component of the momentum equation. The form in which this boundary condition is implemented is important not only because of the overall accuracy, but also because of the efficiency of the numerical scheme. This aspect still has much room for improvement.

Pressure correction methods [8], [10], consist of a basic predictor-corrector procedure between the velocity and the pressure fields. Using an initial approximation of the pressure, the momentum equation can be solved to obtain an intermediate velocity field. This velocity, in general, does not satisfy the divergence-free constraint and must, therefore; be corrected. By taking the divergence of the momentum equation and enforcing the incompressibility constraint, a Poisson equation for the pressure correction (the difference between the new and the old pressure) is obtained. Using the pressure correction, the new velocity field can then be computed. An advantage of the pressure correction technique is that, contrary to the full splitting approach, the final velocity is guaranteed to satisfy the incompressibility constraint; of course, this is only true for the velocity in the continuous (semi-discrete) formulation. A drawback of this approach is that, in order to ensure divergence-freedom, a homogeneous Neumann condition for the Poisson equation for the pressure correction must be used; which clearly is not valid for the pressure itself [20].

In this paper a projection method, related to the pressure correction approach, is given in order to circumvent the above problem concerning the pressure computation [22]. Also, it has been shown that the resulting velocity and pressure satisfy the original Navier–Stokes equations, except for the tangential boundary condition for the velocity, which under certain conditions of smoothness, is satisfied with second-order accuracy in time [22]. For the spatial discretization, a high-order Galerkin spectral element method [15], [20], that exhibits excellent properties (small numerical diffusion and dispersion) for convection-dominated flows is chosen.

The outline of the paper is as follows. Section 2 presents the numerical scheme to solve the Navier–Stokes equations. The equations are first split according to an operator splitting procedure that decouples the treatment of convection and diffusion [16], [21], including the pressure term temporarily in the viscous part of the equations. Next, the velocity treatment is decoupled from the pressure treatment by applying the projection algorithm. In section 3 special attention is given to outflow boundary conditions with respect to the projection scheme. In section 4 the scheme is used to simulate the development of instabilities in a shear-layer flow. Finally, in section 5 conclusions are drawn.

2 Numerical method

2.1 Projection methods

In this section the projection scheme for the Navier–Stokes equations is given. The solution algorithm can be applied either to the continuous or the discrete system of equations. In the latter case, the boundary conditions are already built in directly in the weak or variational formulation, thereby eliminating the need to formulate a specific boundary condition for the discrete pressure Poisson equation. In this case the choice of the element for the velocity and the pressure is important with respect to the well-posedness of the system. As is well-known from the theory of saddle-point of problems, a discrete form of the Brezzi–Babuška condition [1] must then be satisfied for obtaining a unique velocity and pressure. For a high-order spectral element approximation this means that the degree of approximation for the pressure must be taken two degrees lower than that of the velocity [14].

On the other hand, applying the decoupling procedure to the continuous equations leads to a more straightforward scheme, since in that case the original problem is reformulated into several new (and simpler) problems. The theory of saddle-point problems is, then, no longer applicable; as a consequence the degree of approximation for velocity and pressure can be taken to be the same, yielding a simpler-to-implement numerical scheme. In that case however, the resulting Poisson equation requires a boundary condition. It has been shown in [22] that in the continuous projection scheme presented below, the use of a homogeneous Neumann boundary condition for the Poisson equation is valid and, even, essential in obtaining a divergence-free velocity field.

2.2 The projection scheme

Consider the Navier–Stokes equations in primitive variables for incompressible flow in an open and bounded domain Ω with boundary Γ and with, for now, only essential

boundary conditions

$$(1)\quad \begin{cases} \dfrac{\partial \mathbf{u}}{\partial t} + (\mathbf{u}\cdot\nabla)\mathbf{u} - (\nabla\cdot\nu\nabla)\mathbf{u} + \nabla p = \mathbf{f} & \text{in } \Omega, \\ \nabla\cdot\mathbf{u} = 0 & \text{in } \overline{\Omega}, \\ \mathbf{u} = \mathbf{g} & \text{on } \Gamma, \\ \mathbf{u}(\mathbf{x},0) = \mathbf{u}_0 & \text{in } \overline{\Omega}. \end{cases}$$

The first step in the solution method is to apply an operator splitting technique for unsteady convection-diffusion problems, including the pressure term temporarily in the viscous part of the equation. Thereto the momentum equation is written in the following form

$$(2)\qquad \frac{\partial \mathbf{u}}{\partial t} = \mathcal{D}\mathbf{u} + \mathcal{C}\mathbf{u} - \nabla p + \mathbf{f},$$

with $\mathcal{D} = (\nabla\cdot\nu\nabla)$ as the diffusion operator and $\mathcal{C} = -(\mathbf{u}\cdot\nabla)$ as the non-linear convection operator. Equation (2) is written in terms of an integrating factor in $\mathcal{C}$ [16], [21]

$$(3)\qquad \frac{\partial}{\partial t}\left(\mathcal{Q}_{\mathcal{C}}^{(t^*,t)}\mathbf{u}\right) = \mathcal{Q}_{\mathcal{C}}^{(t^*,t)}(\mathcal{D}\mathbf{u} - \nabla p + \mathbf{f}),$$

With $\frac{\partial}{\partial t}\mathcal{Q}^{(t^*,t)} = -\mathcal{Q}^{(t^*,t)}\mathcal{C}$ and $\mathcal{Q}^{(t^*,t^*)} = \mathcal{I}$. The 'Stokes' equation (3) is integrated using an implicit backward differences scheme with time-step Δt [7]. This yields the following semi-discrete system

$$(4)\qquad \frac{\beta_0\mathbf{u}^{n+1} - \sum_{i=1}^{k}\beta_i\mathcal{Q}_{\mathcal{C}}^{(t^{n+1},t^{n+1-i})}\mathbf{u}^{n+1-i}}{\Delta t} = \mathcal{D}\mathbf{u}^{n+1} - \nabla p^{n+1} + \mathbf{f}^{n+1}.$$

To evaluate the terms $\mathcal{Q}_{\mathcal{C}}^{(t^{n+1},t^{n+1-i})}\mathbf{u}^{n+1-i}(i = 1,2,\ldots)$ the following associated initial value problem is solved

$$(5)\qquad \begin{cases} \dfrac{\partial \tilde{\mathbf{u}}(s)}{\partial s} = \mathcal{C}\tilde{\mathbf{u}}(s), \quad 0 < s < i\Delta t, \\ \tilde{\mathbf{u}}(0) = \mathbf{u}^{n+1-i}, \end{cases}$$

from which it follows that

$$(6)\qquad \mathcal{Q}_{\mathcal{C}}^{(t^{n+1},t^{n+1-i})}\mathbf{u}^{n+1-i} = \tilde{\mathbf{u}}(i\Delta t).$$

Problem (5), according to the non-linear convection, is solved using a three-step explicit Taylor–Galerkin scheme also used in [9]. This scheme is, for linear systems, third-order accurate in time. The initial condition is $\tilde{\mathbf{u}}^0 = \mathbf{u}^{n+1-i}$; a time-step Δs such that $\Delta t = j\Delta s$ with j an integer is used. The semi-discrete convection step then becomes

$$(7)\qquad \begin{aligned} \tilde{\mathbf{u}}^{m+\frac{1}{3}} &= \tilde{\mathbf{u}}^m - \frac{\Delta s}{3}(\tilde{\mathbf{u}}^m\cdot\nabla)\tilde{\mathbf{u}}^m, \\ \tilde{\mathbf{u}}^{m+\frac{1}{2}} &= \tilde{\mathbf{u}}^m - \frac{\Delta s}{2}(\tilde{\mathbf{u}}^{m+\frac{1}{3}}\cdot\nabla)\tilde{\mathbf{u}}^{m+\frac{1}{3}}, \\ \tilde{\mathbf{u}}^{m+1} &= \tilde{\mathbf{u}}^m - \Delta s(\tilde{\mathbf{u}}^{m+\frac{1}{2}}\cdot\nabla)\tilde{\mathbf{u}}^{m+\frac{1}{2}}. \end{aligned}$$

After introduction of the simpler notation $\tilde{\mathbf{u}}^{n+1-i} = \mathcal{Q}^{(t^{n+1-i},t^n)}\mathbf{u}^{n+1-i}$ equation (6) leads to

$$(8)\qquad \tilde{\mathbf{u}}^{n+1-i} = \tilde{\mathbf{u}}^{i(j+1)}.$$

For a second-order backward differences scheme, equation (4) reads as follows

$$(9)\quad \begin{cases} \dfrac{3}{2}\mathbf{u}^{n+1} - \Delta t\mathcal{D}\mathbf{u}^{n+1} = 2\tilde{\mathbf{u}}^n - \dfrac{1}{2}\tilde{\mathbf{u}}^{n-1} \\ \qquad -\Delta t\nabla p^{n+1} + \Delta t\mathbf{f}^{n+1} & \text{in } \Omega, \\ \nabla\cdot\mathbf{u}^{n+1} = 0 & \text{in } \overline{\Omega}, \\ \mathbf{u}^{n+1} = \mathbf{g}^{n+1} & \text{on } \Gamma. \end{cases}$$

The projection scheme proceeds as follows (see [22]):

- Calculate an intermediate velocity field $\mathbf{u}^*$ by choosing the pressure at the previous time-level

$$(10)\qquad \begin{aligned} \frac{3}{2}\mathbf{u}^* - \Delta t\mathcal{D}\mathbf{u}^* &= 2\tilde{\mathbf{u}}^n - \frac{1}{2}\tilde{\mathbf{u}}^{n-1} \\ &- \Delta t\nabla p^n + \Delta t\mathbf{f}^{n+1}. \end{aligned}$$

  The intermediate velocity field $\mathbf{u}^*$ is, in general, not divergence-free. The quantities $\tilde{\mathbf{u}}^n$ and $\tilde{\mathbf{u}}^{n-1}$ are calculated according to the convection problem (7), (8).

- The velocity at time-level $n+1$ can be obtained by subtracting (10) from the original momentum equation (9). This yields

$$(11)\qquad \begin{aligned} \frac{3}{2}\frac{\mathbf{u}^{n+1} - \mathbf{u}^*}{\Delta t} &= + \mathcal{D}(\mathbf{u}^{n+1} - \mathbf{u}^*) \\ &- \nabla\left(p^{n+1} - p^n\right). \end{aligned}$$

  A quantity, q, is computed by solving the Poisson equation resulting by taking the divergence of equation (11)

$$(12)\qquad \nabla^2 q = \frac{3}{2}\frac{\nabla\cdot\mathbf{u}^*}{\Delta t}.$$

  with:

$$(13)\qquad q = p^n - p^{n+1} + \nu\nabla\cdot\mathbf{u}^*$$

- According to equation (12) a new velocity satisfying $\nabla\cdot\mathbf{u}^{n+1} = 0$ can be computed from

$$(14)\qquad \mathbf{u}^{n+1} = \mathbf{u}^* - \frac{2}{3}\Delta t\nabla q.$$

- Finally, the pressure at the time-level $n+1$ is computed from (13) as:

$$p^{n+1} = p^n + q - \nu \nabla \cdot \mathbf{u}^*. \tag{15}$$

Some comments on boundary conditions are in order. A general and consistent choice is to adopt for the intermediate velocity $\mathbf{u}^*$ the original boundary conditions at the time-level $n+1$; that is to choose $\mathbf{u}^* = \mathbf{g}^{n+1}$ on $\mathbf{\Gamma}$. Due to the continuous formulation an 'artificial' boundary condition must be formulated for equation (12). In the above scheme a homogeneous Neumann boundary condition arises in a natural way. The solvability constraint for the Poisson equation (12) reads

$$\begin{aligned} \int_{\mathbf{\Omega}} \nabla^2 q \; d\mathbf{\Omega} &= \frac{3}{2\Delta t} \int_{\mathbf{\Omega}} \nabla \cdot \mathbf{u}^* \; d\mathbf{\Omega} \\ &= \frac{3}{2\Delta t} \int_{\mathbf{\Gamma}} \mathbf{n} \cdot \mathbf{u}^* \; d\mathbf{\Gamma} = 0, \end{aligned} \tag{16}$$

due to the global mass constraint and the assumption that $\mathbf{u}^* = \mathbf{g}^{n+1}$ on $\mathbf{\Gamma}$. On the other hand

$$\int_{\mathbf{\Omega}} \nabla^2 q \; d\mathbf{\Omega} = \int_{\mathbf{\Gamma}} \frac{\partial q}{\partial n} \; d\mathbf{\Gamma}. \tag{17}$$

Therefore, the easiest way to satisfy global divergence-freedom is to impose a homogeneous Neumann condition for the Poisson equation (12).

Note that in the projection scheme both the velocity and the pressure are predicted in the first step, and then corrected in the remaining three steps. It can easily be shown that the solution $(\mathbf{u}^{n+1}, p^{n+1})$ of the scheme is consistent with that of the original system (9). Equation (14) also ensures that the normal component of the boundary conditions for $\mathbf{u}^{n+1}$ is satisfied on the boundary; the tangential component of the boundary condition can not be satisfied exactly. However, it can be shown that if the acceleration $\frac{\partial \mathbf{u}}{\partial t}$ on $\mathbf{\Gamma}$ and the source term are continuous in time (sudden starts and sudden sources are not allowed), the tangential boundary condition for the velocity is satisfied with accuracy $\mathcal{O}(\Delta t^2)$ [22], yielding a second-order in time consistent projection scheme.

2.3 Spectral element discretization

Application of a Galerkin spectral element discretization to the semi-discrete projection equations is performed in the standard way. As already stated in section 2.1, there is no need to satisfy any form of the discrete Brezzi–Babuška condition as the decoupling procedure is applied to the continuous equations, leading to uncoupled problems for both velocity and pressure. Therefore, the degree of approximation of the pressure can be taken as equal to that of the velocity, resulting in a numerical algorithm that is simple to implement. The fully discrete form of the projection scheme thus becomes:

- Calculate $\mathbf{u}^*$ by solving

$$\begin{aligned} \left(\frac{3}{2}\mathbf{M} + \Delta t \mathbf{D}\right) \mathbf{u}^* &= 2\mathbf{M}\tilde{\mathbf{u}}^n - \frac{1}{2}\mathbf{M}\tilde{\mathbf{u}}^{n-1} \\ &- \Delta t \mathbf{Q}\mathbf{p}^n + \Delta t \mathbf{M}\mathbf{f}^{n+1}, \end{aligned} \tag{18}$$

with $\mathbf{M}$ the (diagonal) mass matrix, $\mathbf{D}$ the diffusion matrix and $\mathbf{Q}$ the gradient matrix. The column $\mathbf{p}^n$ contains the pressure components at $t = t^n$. The column $\mathbf{f}$ also contains the contribution of non-homogeneous boundary conditions. The columns $\tilde{\mathbf{u}}^n$ and $\tilde{\mathbf{u}}^{n-1}$ are calculated through the solution of

$$\begin{aligned} \tilde{\mathbf{u}}^{m+\frac{1}{3}} &= \tilde{\mathbf{u}}^m - \frac{\Delta s}{3}\mathbf{M}^{-1}\mathbf{C}^m\tilde{\mathbf{u}}^m, \\ \tilde{\mathbf{u}}^{m+\frac{1}{2}} &= \tilde{\mathbf{u}}^m - \frac{\Delta s}{2}\mathbf{M}^{-1}\mathbf{C}^{m+\frac{1}{3}}\tilde{\mathbf{u}}^{m+\frac{1}{3}}, \\ \tilde{\mathbf{u}}^{m+1} &= \tilde{\mathbf{u}}^m - \Delta s \mathbf{M}^{-1}\mathbf{C}^{m+\frac{1}{2}}\tilde{\mathbf{u}}^{m+\frac{1}{2}}, \end{aligned} \tag{19}$$

where $\mathbf{C}^{m+\frac{1}{3}}$ and $\mathbf{C}^{m+\frac{1}{2}}$ denote the convection matrix at time levels $m+\frac{1}{3}$ and $m+\frac{1}{2}$, respectively.

- Calculate $\mathbf{q}$ by solving

$$\mathbf{K}\mathbf{q} = -\frac{3}{2}\frac{\mathbf{L}\mathbf{u}^*}{\Delta t}, \tag{20}$$

with $\mathbf{K}$ as the Laplacian matrix and $\mathbf{L}$ as the divergence matrix.

- Calculate $\mathbf{u}^{n+1}$ via

$$\mathbf{u}^{n+1} = \mathbf{u}^* - \frac{2}{3}\Delta t \mathbf{M}^{-1}\mathbf{Q}\mathbf{q}. \tag{21}$$

- Calculate p^{n+1} via

$$\mathbf{p}^{n+1} = \mathbf{p}^n + \mathbf{q} - \nu \mathbf{M}^{-1}\mathbf{L}\mathbf{u}^*. \tag{22}$$

From the above system it can be seen that it is essential that the mass matrix $\mathbf{M}$ is diagonal, since, then; the equations (19), (21) and (22) do not involve the solution of a system, but only the calculation of matrix-vector products which can be performed on elemental level. For high-order methods the use of a diagonal mass-matrix is a valid approach with respect to accuracy, as is shown numerically in [19].

Note that after spatial discretization divergence-freedom of the final computed velocity is only satisfied in the weak sense. Also, the use of the diagonal mass matrix can further decrease the accuracy with which the incompressibility constraint is satisfied. However, the numerical results presented in [22] suggest that for a high-order method this loss of accuracy is not severe.

3 Outflow boundary conditions

In this section special attention is given to the formulation and implementation of boundary conditions if there is an outflow boundary, as is often the case in numerical flow simulations. The problem of shear-layer flow discussed in the next section also has an outflow boundary. In the case of projection methods the implementation of outflow boundary conditions is not trivial.

Assume, for simplicity, that the outward (normal to the outflow) boundary $\mathbf{\Gamma_\sigma}$ is parallel to the x-axis (in two dimensions). The most commonly used outflow boundary conditions in the context of Galerkin methods read

$$p - \nu\frac{\partial u}{\partial x} = 0 \qquad \text{on } \mathbf{\Gamma_\sigma}, \tag{23}$$

$$\frac{\partial v}{\partial x} = 0 \qquad \text{on } \mathbf{\Gamma_\sigma}, \tag{24}$$

where $\mathbf{u} = (u\ v)^T$. Equations (23), (24) specify zero stress or 'traction free' boundary conditions, which are natural for the weak formulation of the Navier–Stokes equations.

In a formulation where a Poisson equation for the pressure (or a related quantity) has to be solved, as is the case with projection methods, equations (23), (24) are often imposed as

$$p = 0 \qquad \text{on } \mathbf{\Gamma_\sigma}, \tag{25}$$

$$\frac{\partial u}{\partial x} = 0 \qquad \text{on } \mathbf{\Gamma_\sigma}, \tag{26}$$

$$\frac{\partial v}{\partial x} = 0 \qquad \text{on } \mathbf{\Gamma_\sigma}. \tag{27}$$

It can easily be seen, however, that if a strong incompressibility is supposed, condition (27) imposes that the second component of the velocity be zero at the outlet, which is too strong [13]. Therefore, this possibility is not considered here.

The projection method used in this paper involves equations in terms of an intermediate velocity $\mathbf{u}^*$ and a quantity q related to the pressure. Therefore, equations (23), (24) must be reformulated in order to obtain conditions on these variables. Equation (23) implies on the time-level $n+1$

$$p^{n+1} - \nu\frac{\partial u^{n+1}}{\partial x} = 0 \qquad \text{on } \mathbf{\Gamma_\sigma}. \tag{28}$$

Using equations (12), (14) of the projection scheme, the second term in this equation can be written as

$$\begin{aligned} \nu\frac{\partial u^{n+1}}{\partial x} &= \nu\left(\frac{\partial u^*}{\partial x} - \frac{2}{3}\Delta t\frac{\partial^2 q}{\partial x^2}\right) \\ &= \nu\frac{\partial u^*}{\partial x} - \frac{2}{3}\Delta t\nu\left(\frac{\partial^2 q}{\partial y^2} - \frac{3}{2}\frac{\nabla\cdot u^*}{\Delta t}\right), \end{aligned} \tag{29}$$

on the outflow boundary $\mathbf{\Gamma_\sigma}$. Combining equation (29) with equation (15) yields

$$p^n + q - \nu\frac{\partial u^*}{\partial x} - \frac{2}{3}\Delta t\nu\frac{\partial^2 q}{\partial y^2} = 0. \tag{30}$$

Next, if the natural boundary condition for the Helmholtz equation (10) for $\mathbf{u}^*$, which reads

$$p^n - \nu\frac{\partial u^*}{\partial x} = 0 \qquad \text{on } \mathbf{\Gamma_\sigma} \tag{31}$$

is imposed, it follows that

$$q - \frac{2}{3}\Delta t\nu\frac{\partial^2 q}{\partial y^2} = 0 \qquad \text{on } \mathbf{\Gamma_\sigma}. \tag{32}$$

This admits the solution

$$q = 0 \qquad \text{on } \mathbf{\Gamma_\sigma}. \tag{33}$$

So, it is valid to use equations (31) and (33), which in a strong sense ensure that equation (23)is satisfied.

Finally, using equation (14) the condition (24) can be reformulated as

$$\frac{\partial v^*}{\partial x} - \frac{2}{3}\Delta t\frac{\partial}{\partial x}\left(\frac{\partial q}{\partial y}\right) = 0 \qquad \text{on } \mathbf{\Gamma_\sigma}. \tag{34}$$

If it is assumed that $q = q_1(t)q_2(x,y)$ (which is the case with the spatial discretization used), it can be shown [22] that $q = \mathcal{O}(\Delta t)$ and, therefore; that the the second term in (34) is $\mathcal{O}(\Delta t^2)$. Thus, without loss of the second-order accuracy $\frac{\partial v^*}{\partial x} = 0$ implies that $\frac{\partial v^{n+1}}{\partial x} = 0$ which ensures that equation (24) is also satisfied.

4 Shear-layer flow

Consider a mixing-layer in the (x,y)-plane in the domain $0 \le x \le 8, -0.5 \le y \le 0.5$. At $t = 0$ the velocity and pressure fields are set to zero. The boundary conditions at the inlet, top and bottom boundaries, read

$$u(y,t) = \hat{u}(t)\left(1 + 0.5\tanh\frac{y}{\delta}\right), \tag{35}$$

with $\delta = 0.005$. In order to ensure a smooth start-up the velocity $\hat{u}(t)$ is smoothly increased for $0 \leq t \leq 1$ as

$$\hat{u}(t) = 0.5\,(1 - \cos(2\pi t))\,, \tag{36}$$

and from $t = 1$ on set to 1. At the outlet, stress-free outflow conditions are described. The formulation of these conditions is discussed in the previous section.

In Figure 1 the streamlines are shown of the computed velocity field at time-levels $t = 2, 6, 10, 14, 18$ on a mesh of 12×8 spectral elements of order 8. The viscosity ν is take such that the Reynolds number based on the distance between the upper and lower walls equals $Re = 1000$. The results seem to be fair: during the initial transience ($t \leq 1$) the flow spontaneously sheds a travelling wave which is amplified and convected through the whole domain. In order to get a clearer (and more honest) picture of the flow it is visualized by convecting a scalar field c (for example the color) with the flow using the three-step explicit scheme for the non-linear convection step of the projection method, see equation (7). Initially, c is set to y, and the boundary condition $c = y$ at $x = 0$ is imposed. This representation of the flow can be seen in Figure 2 where plots of the scalar field c are given, again at time-levels $t = 2, 6, 10, 14, 18$.

It is clear from Figure 2 that especially around the inter-elemental boundaries some wiggles are created. These results seem to indicate that further numerical experiments with a stabilized scheme for the convection may be useful for these kind of stability studies. Also, for this scalar convection the mesh consists of only 12×8 elements of degree 8. Although sufficient for the total flow problem (see below) this may not be enough for the pure convection problem. Nevertheless, the whole picture of the instability development is adequately represented.

In order to examine the influence of the mesh on the total flow problem computations are also performed using 8×8 and 16×8 elements of degree 8. All meshes are sufficiently refined around the line $y = 0$ and at the inlet.

Figure 3 shows the time-series of the second component of the velocity at the point $(x, y) = (4.1, 0)$. The results of the computations using 12×8 and 16×8 elements are absolutely comparable. The result of the computation using 8×8 elements, however, is qualitatively different. In the case of the fine meshes the initial spontaneous shedding is damped, and for $t > 50$ the flow is practically steady. This region is, therefore, not shown nor computed. In the case of the coarser mesh the time-series represents a quasi-steady periodic flow. The power spectrum of the signal, given in Figure 1, shows a single frequency of about 0.7. These results seem to confirm [6], [17], that if the mesh of spectral elements used is not sufficiently fine, spurious oscillations can be created which resemble a periodic regime.

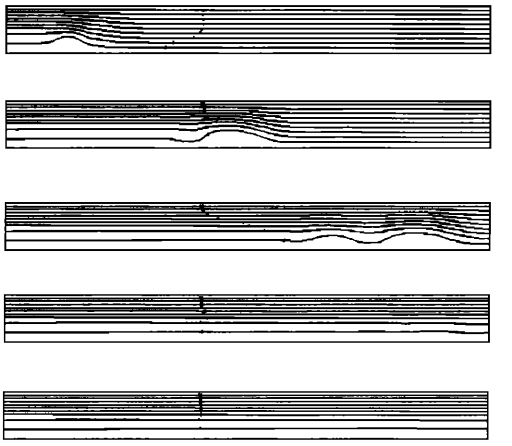

Figure 1: Streamlines of computed velocity field at time-levels: $t = 2, 6, 10, 14, 18$ (top to bottom).

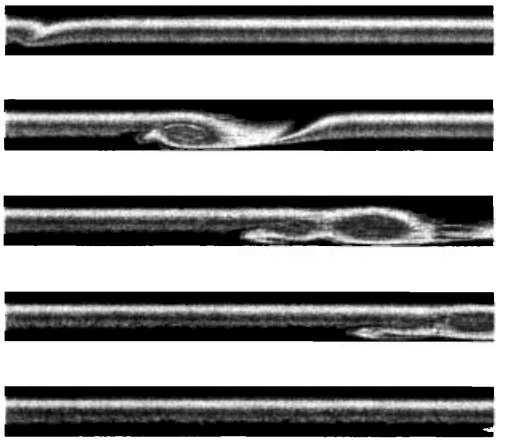

Figure 2: Representation of the computed flow field by passive scalar convection at time-levels: $t = 2, 6, 10, 14, 18$ (top to bottom).

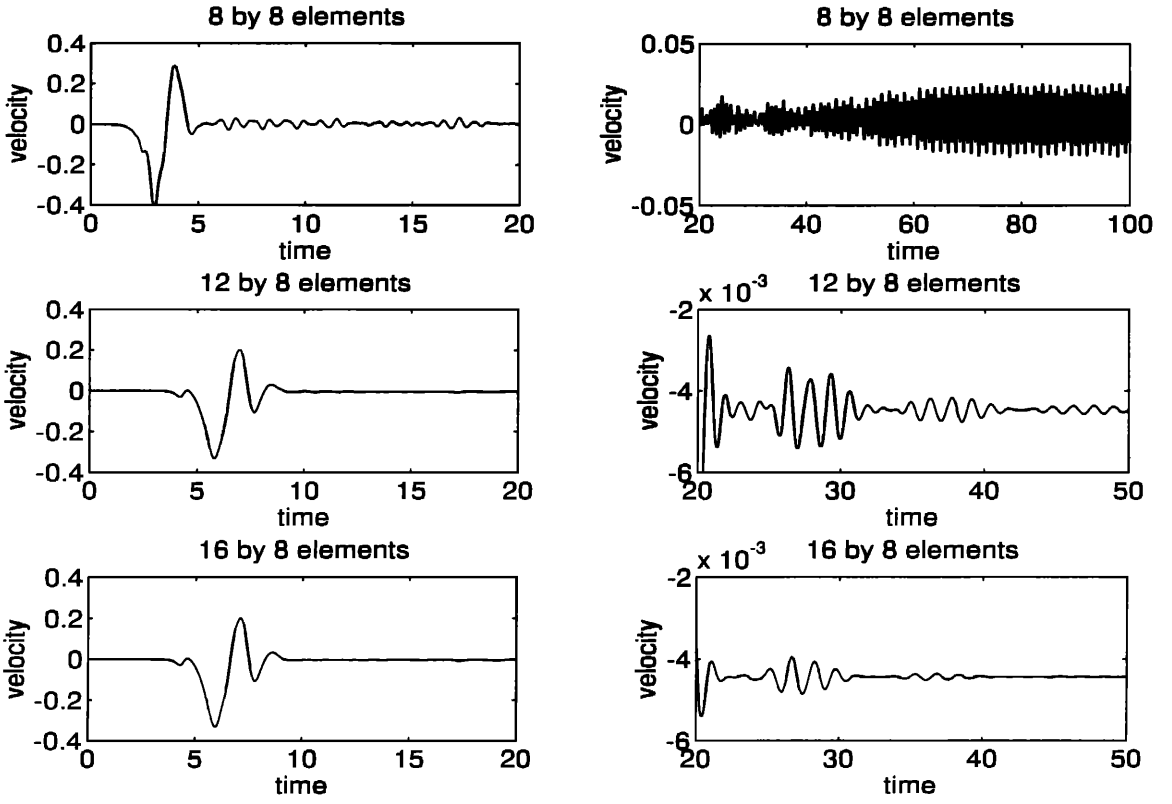

Figure 3: Time-series of the second component of the computed velocity at location $(x, y) = (4.1, 0)$ for three different meshes. The left column contains the time history up till $t = 20$ the right column contains the time history from $t = 20$ on.

5 Conclusions

A spectral element projection scheme for the Navier-Stokes equations is discussed. The main advantage of this method is that it allows the reformulation of the system into another one consisting of two Helmholtz (three in the 3-D case) equations and one Poisson equation. The last set can be solved relatively effectively without the necessity of introducing an additional iteration loop (as it is the case with the Uzawa-like algorithms) by means of a direct or iterative method. A second advantage is that this scheme suggests an easy and consistent choice of no-slip boundary conditions for the intermediate velocity ($\mathbf{u}^*$ in our notation) and the intermediate pressure correction (q in our notation) boundary condition. Moreover, it can be shown [22] that under some smoothness conditions for the acceleration $\partial \mathbf{u}/\partial t$ on Γ the resulting velocity and pressure satisfy the original coupled system up to an $O(\Delta t^2)$ error in the tangential boundary condition for the velocity.

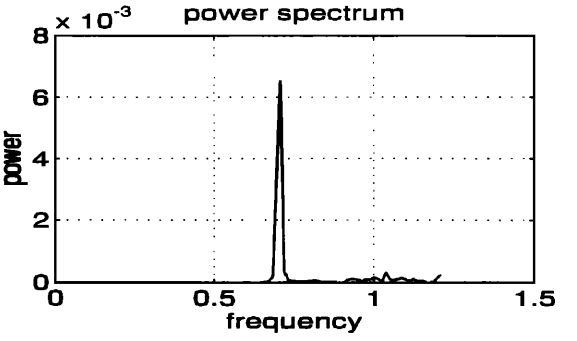

Figure 4: Power spectrum of the time-series of the second component of the computed velocity at location $(x, y) = (4.1, 0)$ for 8×8 elements.

A set of free-outlet boundary conditions in terms of the new variables ($\mathbf{u}^*$ and q) is derived, too. The computations show that these outflow conditions are not too restrictive and allow the convection of vortices out of the computational domain.

The scheme discussed above is validated, simulating the development of instability in a shear layer. It is shown that the insufficient resolution of the spectral element mesh can cause spurious oscillations in the flow which can be erroneously interpreted as oscillations of a physical origin. The flow pattern is visualized by a convection of an initially given passive scalar field. Using the same space and time discretization as for the convective part of the Navier–Stokes equations, it yields acceptable results on a relatively coarse mesh without the introduction of an artificial dissipation. The presence of low-amplitude but spurious oscillations in this scalar field, however, indicates that even the finest spectral element mesh used in this study may not be fine enough to resolve all the details of the flow field.

References

[1] F. Brezzi, *On the existence, uniqueness and approximation of saddle-point problems arising from Lagrangian multipliers*, RAIRO, 8 (1974), pp. 129-151.

[2] A.J. Chorin, *Numerical solution of the Navier–Stokes equations*, Math. Comp., 22 (1968). pp. 745-761.

[3] V. Girault and P.A. Raviart, Finite element methods for Navier–Stokes equations, Springer–Verlag, New York, Berlin, 1986.

[4] P.M. Gresho and R.L. Sani, *On pressure boundary conditions for the incompressible Navier-Stokes equations*, Int. J. Numer. Meth. Fluids, 7 (1987), pp. 1111-1145.

[5] P.M. Gresho, *On the theory of semi-implicit projection methods for viscous incompressible flow and its implementation via a finite element method that also introduces a nearly consistent mass matrix. Part 1: Theory*, Int. J. Numer. Meth. Fluids, 11 (1990), pp. 587-620.

[6] P.M. Gresho, D.K. Gartling, J.R. Torczynski, K.A. Cliffe, K.H. Winters, T.J. Garratt, A. Spence and J.W. Goodrich, *Is the steady viscous incompressible two-dimensional flow over a backward-facing step at Re = 800 stable?*, Int. J. Numer. Meth. Fluids, 17 (1993), pp. 501-541.

[7] E. Hairer, G. Wanner and S.P. Noersett, Solving ordinary differential equations I. Nonstiff problems, Springer, Berlin, 1987.

[8] D.M. Hawken, H.R. Tamaddon-Jahromi, P. Townsend and M.F. Webster, *A Taylor-Galerkin based algorithm for viscous incompressible flow*, Int. J. Numer. Meth. Fluids, 10 (1990), pp. 327-351.

[9] C.B. Jiang and M. Kawahara, *A three-step finite element method for unsteady incompressible flows*, Comp. Mech., 11 (1993), pp. 355-370.

[10] J. van Kan, *A second-order accurate pressure-correction scheme for viscous incompressible flow*, SIAM J. Sci. Stat. Comp., 7 (1986), pp. 870-891. 87 (1991), pp. 201-252.

[11] G.E. Karniadakis, M. Israeli and S.A. Orszag S.A., *High-order splitting schemes for the incompressible Navier–Stokes equations*, J. Comp. Phys., 97 (1991), pp. 414-443.

[12] H. Laval and L. Quartapelle, *A fractional-step Taylor–Galerkin method for unsteady incompressible flows*, Int. J. Numer. Meth. Fluids, 11 (1990), pp. 501-513.

[13] J.M. Leone and P.M. Gresho, *Finite element simulations of steady, two-dimensional viscous incompressible flow over a step*, J. Comp. Phys., 41 (1981), pp. 167-191.

[14] Y. Maday, A.T. Patera and E.M. Rønquist, *A well-posed optimal spectral element approximation for the Stokes problem*, ICASE Report, 87-48, NASA Langley Research Center, Hampton Virginia, 1987.

[15] Y. Maday and A.T. Patera, *Spectral element methods for the incompressible Navier–Stokes equations*, in A. Noor (ed.), State-of-the-Art surveys on computational mechanics, ASME, New York, 1989, pp. 71-143.

[16] Y. Maday, A.T. Patera and E.M. Rønquist, *An operator-integration-factor splitting method for time-dependent problems: application to incompressible fluid flow*, J. Sci. Comp., 5 (1990), pp. 263-292.

[17] P.D. Minev, F.N. van de Vosse, L.J.P. Timmermans and A.A. van Steenhoven, *A second order splitting algorithm for thermally-driven flow problems*, accepted in Int. J. Num. Meth. Heat & Fluid Flow.

[18] S.A. Orszag, M. Israeli and M.O. Deville, *Boundary conditions for incompressible flows*, J. Sci. Comp., 1 (1986), pp. 75-111.

[19] L.J.P. Timmermans and F.N. van de Vosse, *Spectral methods for advection-diffusion problems*, in C.B. Vreugdenhil and B. Koren (eds.), Notes on numerical fluid mechanics: numerical methods for advection-diffusion problems, Vieweg, Braunschweig, 1993, pp. 171-194.

[20] L.J.P. Timmermans, Analysis of spectral element methods with application to incompressible flow, Ph.D. Thesis, Eindhoven University of Technology, Eindhoven, 1994.

[21] L.J.P. Timmermans, F.N. van de Vosse and P.D. Minev, *Taylor–Galerkin based spectral element methods for convection-diffusion problems*, Int. J. Numer. Meth. Fluids, 18 (1994), pp. 853-870.

[22] L.J.P. Timmermans, P.D. Minev and F.N. van de Vosse, *An approximate projection scheme for incompressible flow using spectral elements*, accepted for publication in Int. J. Numer. Meth. Fluids (1995).